J. theor. Biol. (1998) **195,** 69–85
Article No. jt980781

Bifurcation Analysis of a Model of Mitotic Control in Frog Eggs

MARK T. BORISUK AND JOHN J. TYSON*

Department of Biology, Virginia Polytechnic Institute and State University, Blacksburg, VA 24061, *U.S.A.*

(*Received on* 13 *March* 1998, *Accepted in revised form on* 7 *July* 1998)

Novak and Tyson have proposed a realistic mathematical model of the biochemical mechanism that regulates M-phase promoting factor (MPF), the major enzymatic activity controlling mitotic cycles in frog eggs, early embryos, and cell-free egg extracts. We use bifurcation theory and numerical methods (AUTO) to characterize the codimension-one and -two bifurcation sets in this model. Our primary bifurcation parameter is the rate constant for cyclin synthesis, which can be manipulated experimentally by adding exogenously synthesized cyclin mRNA to extracts depleted of all endogenous mRNA molecules. For the secondary bifurcation parameter we use the total amount of one of the principal regulatory enzymes in the extract (APC, the enzyme complex that labels cyclin for degradation; Wee1, the kinase that inhibits MPF; or Cdc25, the phosphatase that activates MPF). We find a rich array of physiologically distinct behaviors exhibited by the model as these parameters are varied around values that seem plausible for frog eggs and extracts. In addition to unique, stable steady states (cell cycle arrest) and limit cycle oscillations (autonomous, periodic cell division), we find parameter combinations where the control system is bistable. For instance, an interphase-arrested state may coexist with a metaphase-arrested state, or two stable limit cycles of different amplitude and period may coexist. We suggest that such strange behavior is nearly unavoidable in a complex regulatory system like the cell cycle. Perhaps cells exploit some of these exotic bifurcations for control purposes that are as yet unrecognized by physiologists.

1. Introduction

1.1. THE CELL CYCLE

The cell cycle is the sequence of events by which a growing cell duplicates all its components and then divides this material between two daughter cells so that they can repeat the process. The development and reproduction of all living organisms is based on this fundamental ability of a cell to replicate itself. Although there are many unique features of cell proliferation in different organisms, the basic events of the eukaryotic division cycle are stereotypical: first, the DNA molecule within each chromosome is faithfully replicated during S phase (''synthesis''), and then one copy of each DNA molecule is segregated to each sister cell during M phase (''mitosis''). S and M phases alternate in time, in response to signals from a network of enzymatic reactions that is highly conserved across all eukaryotic lineages, from fungi and plants to insects and mammals. In this paper we shall concentrate on cell cycle regulation in frog eggs and early embryos, where the control system is exceptionally simple.

Excellent summaries of the physiology and molecular biology of the eukaryotic cell cycle can

*Author to whom correspondence should be addressed.

0022–5193/98/021069 + 17 $30.00/0

be found in Alberts *et al*. (1994), Lodish *et al*. (1995), Murray & Hunt (1993). These references may be consulted for confirmation of the basic facts gathered in this introduction.

1.2. FROG EGGS

As frog eggs develop (Fig. 1), they grow to about 1 mm diameter and arrest, with replicated DNA, before the first meiotic division. In this state, they are known as immature oocytes. Exposure to hormone (progesterone) triggers immature oocytes to undergo two meiotic divisions, generating mature eggs arrested at metaphase of meiosis II. After fertilization, the egg nucleus completes meiosis II and fuses with the sperm nucleus to create a zygote. The zygote undergoes 12 rapid, synchronous mitotic cycles to form a hollow ball of 4096 cells. At this stage (called the midblastula transition), cell division in the embryo slows down and becomes asynchronous, and major changes occur in mRNA expression.

We are concerned in this paper with regulation of the meiotic and mitotic divisions from egg maturation to the midblastula transition. These divisions are triggered by M-phase promoting factor (MPF), a protein kinase consisting of two subunits: Cdc2 (the catalytic subunit) and cyclin B (the regulatory subunit). (“Cdc2” is also known as “Cdk1”.) When activated, MPF phosphorylates an array of proteins involved in chromosome condensation, nuclear envelope breakdown, spindle formation, and other events of meiosis and mitosis. (In particular, MPF can be assayed biochemically by its ability to phosphorylate histone H1, a DNA-binding protein abundant in chromosomes). As cells exit M phase, MPF activity drops and DNA is permitted to replicate. Thus, during egg maturation and early embryonic cell divisions, the alternation of S and M phases is controlled by temporal fluctuations in MPF activity.

1.3. MPF REGULATION

There are two primary modes of regulation of MPF activity in frog eggs. (1) Although Cdc2 is present at constant level throughout the cell division cycle, its partner fluctuates dramatically

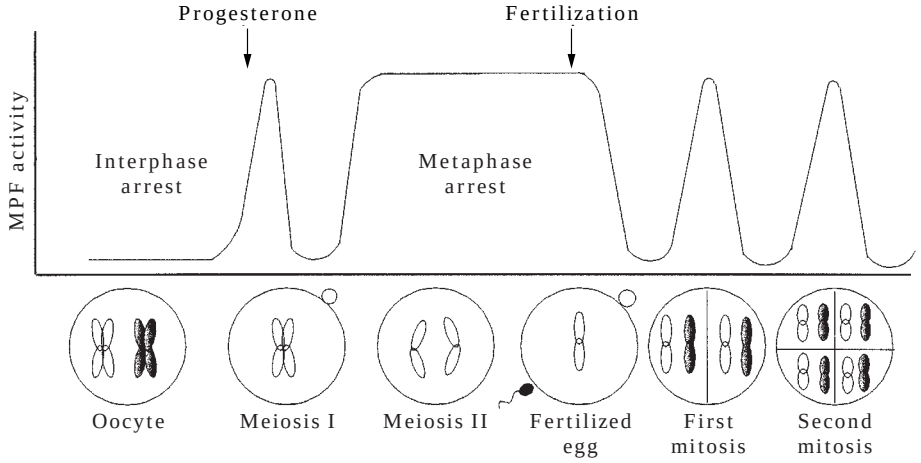

FIG. 1. MPF fluctuations in the meiotic and mitotic cycles of frog eggs (adapted from Murray & Hunt, 1993, Fig. 2–6). The immature oocyte (far left) is arrested in G2 phase with low MPF activity and replicated chromosomes in homologous pairs (the **X**-shaped symbols represent one pair of homologous chromosomes: the two arms of each **X** represent identical DNA molecules called sister chromatids). Progesterone-induced activation of MPF triggers meiosis I, during which homologous chromosomes line up on the spindle. The paired chromosomes are separated to the two poles of the spindle as MPF activity drops at the end of meiosis I. One set of chromosomes remains in the egg and the other set is discarded in a small polar body. As MPF activity rises again, the egg enters meiosis II, with its replicated chromosomes attached again to the spindle. The mature egg arrests in this state, awaiting fertilization. Sperm entry triggers destruction of MPF in the egg, coincident with separation of sister chromatids to the two poles of the spindle. One set of chromatids is discarded in a small polar body, and the other set combines with sperm chromatids to reconstitute the diploid state in the fertilized egg (homologous pairs of unreplicated chromosomes, represented by the **I**-shaped symbols, one from the egg and one from the sperm). Shortly thereafter, the DNA in each chromosome is replicated (they become **X**-shaped, not shown) and about 90 min after fertilization the egg is driven into mitosis 1 by rising MPF activity. Subsequent cycles of MPF activation and inactivation drive a series of rapid, synchronous mitotic divisions to produce a hollow ball of cells, called the blastula.

due to changes in the rate of degradation of cyclin B. Since Cdc2 is catalytically active only when bound to cyclin, MPF activity comes and goes with phases of net cyclin synthesis and degradation. (2) MPF activity can be modified by phosphorylation of the Cdc2 subunit. To be catalytically active, Cdc2 must be phosphorylated at a specific amino acid (threonine at position 161), whereas phosphorylation of a different amino acid (tyrosine at position 15) inhibits Cdc2.

In the mature egg, arrested at metaphase of meiosis II, MPF activity is high because cyclin degradation is repressed. At fertilization, cyclin degradation is derepressed, and MPF activity drops as cyclin is destroyed. The following 12 mitotic cycles are driven by cytoplasmic reactions that periodically activate and inactivate MPF by cyclin turnover and Cdc2 phosphorylation, resulting in MPF activity being low in interphase (the period between subsequent M phases, when DNA is being synthesized) and high in mitosis.

1.4. FROG EGG EXTRACTS

These reactions can be studied conveniently in extracts prepared from mature eggs (Murray & Kirschner, 1989). After crushing the eggs, their cytoplasmic components are separated by low-speed centrifugation from lipids and membranous debris. Calcium ions, liberated from organelles during the extraction procedure, release the arrest on cyclin degradation, and spontaneous oscillations of MPF activity ensue. MPF oscillations in the extract can be observed by adding sperm nuclei, which undergo periodic mitoses whenever MPF activity is high. The inter-mitotic period in extracts (about 60 min) is longer than the period in intact eggs (about 30 min). In extracts, Cdc2 is extensively tyrosine-phosphorylated during interphase, whereas in intact eggs it is not (Ferrell *et al*., 1991).

Biochemical manipulation of the extract can be used to explore properties of the underlying mitotic control system (Murray & Kirschner, 1989). For example, addition of cycloheximide blocks all protein synthesis and prevents MPF oscillations because cyclin cannot be made. Exogenously synthesized cyclin can be added to the cycloheximide-blocked extract to reconstitute MPF activity and drive indicator nuclei into mitosis. Another classic experimental protocol (Murray & Kirschner, 1989) is to destroy all endogenous mRNA in the extract (this kills MPF oscillations because the extract cannot synthesize cyclin) and then add back exogenously produced mRNA for cyclin B. In this way the rate of cyclin synthesis in the extract can be controlled with some precision. If a sufficient quantity of cyclin mRNA is added back, MPF oscillations resume. This proves that cyclin B synthesis is sufficient to drive the early embryonic cell cycle.

1.5. MOLECULAR MECHANISM FOR MPF REGULATION

Biochemical investigations of frog egg extracts, supplemented by genetic observations in yeast, have led to a consensus picture of the molecular mechanism regulating MPF activity (Fig. 2). The mechanism consists of reactions governing phosphorylation and dephosphorylation of Cdc2 and activation of the Anaphase Promoting Complex (APC). The APC attaches ubiquitin moieties to cyclin B, and polyubiquitinated cyclin B is then rapidly degraded. (The APC is also known as the ''cyclosome'' because of its involvement in cyclin degradation).

This mechanism has been converted into a set of nonlinear ordinary differential equations (Table 1) by Novak & Tyson (1993a), who used the model to explain many physiological and biochemical characteristics of mitotic control in intact frog eggs and extracts. Novak & Tyson (1993a, b) found solutions relevant to four observed physiological states:

1. steady state with low MPF activity (cf. immature oocyte);
2. steady state with high MPF activity (cf. mature egg);
3. limit cycle with extensive tyrosine phosphorylation of Cdc2 in interphase (cf. oscillating extract);
4. limit cycle with little tyrosine phosphorylation of Cdc2 (cf. early embryo).

Naturally we might ask whether there are other types of solutions to the underlying differential equations which correspond to other physiological states as yet undiscovered. In this paper we use bifurcation theory to characterize

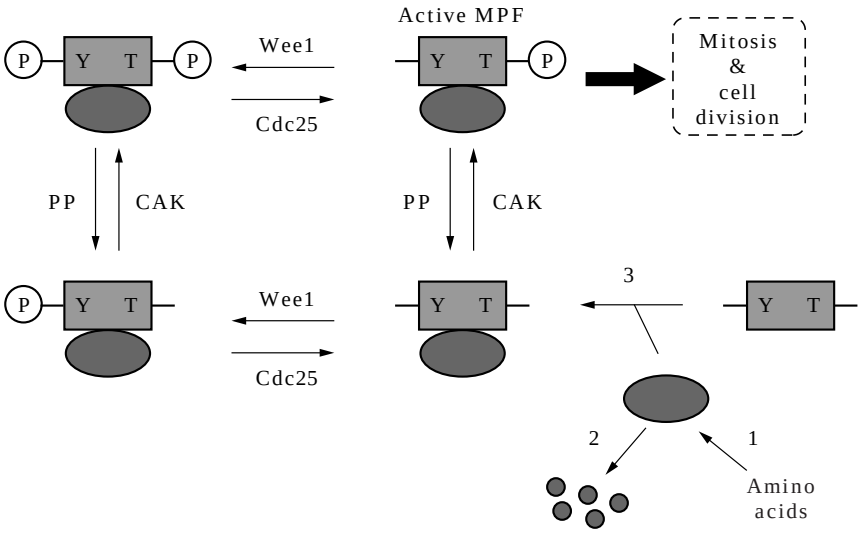

(a) The phosphorylation states of MPF

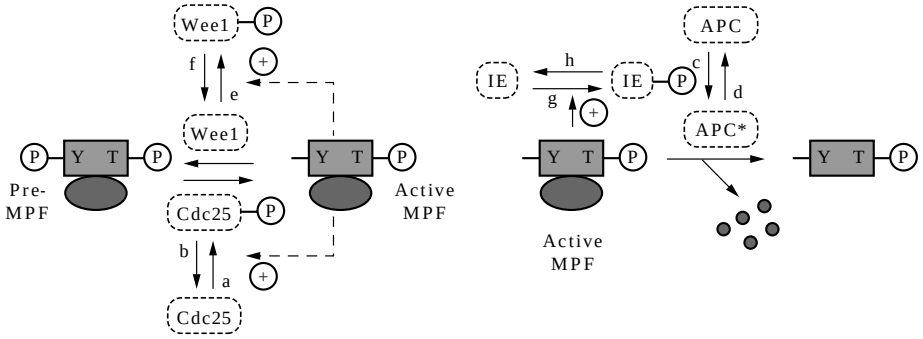

(b) Positive feedback loops (c) Negative feedback loop

FIG. 2. A model of the cell cycle engine in frog eggs (adapted from Novak & Tyson, 1993a, Fig. 1). (a) The dimer box. Oval = cyclin, rectangle = Cdc2, Y = tyrosine-15, T = threonine-161. Weel and Cdc2 are the kinase and phosphatase that operate on tyrosine-15. CAK is the threonine kinase; its opposing phosphatase (PP) is unknown at this time. Active MPF is the dimer in the upper right corner of the box. (b) Wee1 is inactivated and Cdc25 is activated by phosphorylation. Active MPF promotes these phosphorylation steps directly or indirectly. (c) Cyclin degradation is initiated by the anaphase promoting complex (APC). MPF activates APC indirectly, as represented by phosphorylation of an intermediary enzyme (IE). IE could be the *cdc*20 gene product, whose role in cyclin degradation is currently being delineated.

the qualitatively different solutions of the Novak–Tyson model, in order to determine the range of physiologically distinct behaviors available to the control system. In addition to determining how solutions 1–4 are related to each other, we find new solutions that predict unusual responses never before observed in eggs or extracts. The theory suggests many novel experimental tests of the underlying mechanism.

A preliminary version of this work, with more mathematical details, can be found in the first author's dissertation (Borisuk, 1997).

2. One-parameter Bifurcation Diagrams

The differential equations (DEs) in Table 1 determine the temporal behavior of the MPF regulatory network in Fig. 2. An instantaneous state of the network can be thought of as a point in multidimensional phase space (one coordinate for each time-dependent variable in the model), and a solution of the DEs can be represented by a trajectory of state points traced through phase space as time proceeds (Odell, 1980; Segel, 1984; Edelstein-Keshet, 1988; Kaplan & Glass, 1995). A collection of representative solution trajec-

tories in phase space sketches out the phase portrait of the system. As parameter values of the model (Table 2) are changed, the phase portrait may undergo a dramatic qualitative change. For instance, a steady-state solution (a single point in phase space, corresponding to an arrested extract) may lose stability and be replaced by a stable limit cycle solution (a closed curve in phase space, corresponding to periodic activation of MPF). In such cases, we say the system has undergone a bifurcation. (For readers who are unfamiliar with bifurcation theory, we provide a primer of the basic ideas and jargon in the Appendix.) Our intent is to characterize the kinds of qualitative changes that may occur in phase portraits of the Novak–Tyson model as representative biochemical parameters are changed.

To this end we first construct a one-parameter bifurcation diagram (Fig. 3), choosing MPF activity to represent the behavior of the system and k_1, the rate constant for cyclin synthesis, as a particularly important, experimentally adjustable parameter. [The diagram is created by a powerful computer program, AUTO, written by E. Doedel (Doedel & Wang, 1995).] In the figure we plot representative values of MPF activity as k_1 is varied. For k_1 greater than about 0.2 min^{-1}, there exists a single stable steady-state solution, and all initial conditions lead eventually (as $t \to \infty$) to this steady state. The activity of MPF at the steady state is plotted as a solid line for $k_1 > 0.2$ (hereafter it is understood that k_1 carries units min^{-1}). For k_1 somewhat less than 0.2, this steady-state solution has lost stability (now represented by a dashed line), and the only stable

TABLE 1

Novak–Tyson model of MPF regulation in frog eggs

$$\frac{\mathrm{d}[\bigcirc]}{\mathrm{d}t} = k_1[\text{amino acids}] - k_2[\bigcirc] - k_3[\bigcirc][\square]$$

$$\mathrm{d}[[\text{Dimer}]]\mathrm{d}t = k_{PP}[[\text{Dimer}]\text{P}] - (k_{wee} + k_{CAK} + k_2)[[\text{Dimer}]] + k_{25}[\text{P}[\text{Dimer}]] + k_3[\bigcirc][\square]$$

$$\frac{\mathrm{d}[\text{P}[\text{Dimer}]]}{\mathrm{d}t} = k_{wee}[[\text{Dimer}]] - (k_{25} + k_{CAK} + k_2)[\text{P}[\text{Dimer}]] + k_{PP}[\text{P}[\text{Dimer}]\text{P}]$$

$$\frac{\mathrm{d}[\text{P}[\text{Dimer}]\text{P}]}{\mathrm{d}t} = k_{wee}[[\text{Dimer}]\text{P}] - (k_{PP} + k_{25} + k_2)[\text{P}[\text{Dimer}]\text{P}] + k_{CAK}[\text{P}[\text{Dimer}]]$$

$$\frac{\mathrm{d}[[\text{Dimer}]\text{P}]}{\mathrm{d}t} = k_{CAK}[[\text{Dimer}]] - (k_{PP} + k_{wee} + k_2)[[\text{Dimer}]\text{P}] + k_{25}[\text{P}[\text{Dimer}]\text{P}]$$

$$\frac{\mathrm{d}[\text{Cdc25P}]}{\mathrm{d}t} = \frac{k_a[\text{MPF}][\text{total Cdc25}] - [\text{Cdc25P}])}{K_a + [\text{total Cdc25}] - [\text{Cdc25P}]} - \frac{k_b[\text{PPase}][\text{Cdc25P}]}{K_b + [\text{Cdc25P}]}$$

$$\frac{\mathrm{d}[\text{Wee1P}]}{\mathrm{d}t} = \frac{k_e[\text{MPF}][\text{total Wee1}] - [\text{Wee1P}])}{K_e + [\text{total Wee1}] - [\text{Wee1P}]} - \frac{k_f[\text{PPase}][\text{Wee1P}]}{K_f + [\text{Wee1P}]}$$

$$\frac{\mathrm{d}[\text{IEP}]}{\mathrm{d}t} = \frac{k_g[\text{MPF}]([\text{total IE}] - [\text{IEP}])}{K_g + [\text{total IE}] - [\text{IEP}]} - \frac{k_h[\text{PPase}][\text{IEP}]}{K_h + [\text{IEP}]}$$

$$\frac{\mathrm{d}[\text{APC*}]}{\mathrm{d}t} = \frac{k_c[\text{IEP}]([\text{total APC}] - [\text{APC*}])}{K_c + [\text{total APC}] - [\text{APC*}]} - \frac{k_d[\text{anti-IE}][\text{APC*}]}{K_d + [\text{APC*}]}$$

$$k_{25} = V_{25'}([\text{total Cdc25}] - [\text{Cdc25P}]) + V_{25''}[\text{Cdc25P}]$$

$$k_{wee} = V_{Wee'}[\text{Wee1P}] + V_{Wee''}([\text{total Wee1}] - [\text{Wee1P}])$$

$$k_2 = V_{2'}([\text{total APC}] - [\text{APC*}]) + V_{2''}[\text{APC*}]$$

Notes: We write a differential equation for the concentration (or relative activity) of each of the nine regulatory proteins in Fig. 2. The right hand side of each DE has the form *synthesis–degradation + activation–inhibition*. The k_is are rate constants and the K_js are Michaelis constants. The total concentrations of Cdc2, Cdc25, Wee1, APC and IE are all taken to be constant. $V_{i'}$ (resp. $V_{i''}$) is the turnover number for the less active (more active) form of each enzyme.

TABLE 2
Parameter values used in the Novak–Tyson model

	1993	1998
These parameters are dimensionless		
K_a/[total Cdc25]	0.1	0.1
K_b/[total Cdc25]	0.1	1.0
K_c/[total APC]	0.01	0.01
K_d/[total APC]	0.01	1.0
K_e/[total Wee1]	0.3	0.1
K_f/[total Wee1]	0.3	1.0
K_g/[total IE]	0.01	0.01
K_h/[total IE]	0.01	0.01
These parameters have units min^{-1}		
k_1[amino acids]/[total Cdc2]	0.1	0.01
k_3[total Cdc2]	1.0	0.5
V_2[total APC]	0.015	0.005
$V_{2'}$[total APC]	1.0	0.25
V_{25}[total Cdc25]	0.1	0.017
$V_{25'}$[total Cdc25]	2.0	0.17
V_{wee}[total Wee1]	0.1	0.01
$V_{wee'}$[total Wee1]	1.0	1.0
k_{CAK}	0.25	0.64
k_{PP}	0.025	0.004
k_a[total Cdc2]/[total Cdc25]	1.0	2.0
k_b[PPase]/[total Cdc25]	0.125	0.1
k_c[total IE]/[total APC]	0.1	0.13
k_d[anti IE]/[total APC]	0.095	0.13
k_e[total Cdc2]/[total Wee1]	1.33	2.0
k_f[PPase]/[total Wee1]	0.1	0.1
k_g[total Cdc2]/[total IE]	0.65	2.0
k_h[PPase]/[total IE]	0.087	0.15

Notes: The "1993" parameter set is from Novak & Tyson (1993a), the "1998" set is from Marlovits *et al*. (1998).

self-perpetuating solution of the DEs is an oscillatory state, for which MPF activity fluctuates periodically between maximum and minimum values represented by the filled circles on the diagram.

The value of k_1 where the steady state loses stability and is replaced by a stable limit cycle oscillation is called a supercritical Hopf bifurcation point, $k_1^H = 0.18226$. As k_1 is decreased slightly below the bifurcation point, the period of oscillation stays nearly constant and the amplitude of oscillation (max MPF activity–min MPF activity) increases in proportion to $\sqrt{k_1^H - k_1}$.

As the rate of cyclin synthesis is decreased further, we find that the stable periodic solution persists to very small values of k_1. Its period is roughly constant at 35–40 min until k_1 drops below about 0.03, after which the period of oscillation increases rapidly and the oscillatory solution disappears at $k_1^{SNIC} = 0.0040975$ [see Fig. 3(b)]. This point has the characteristics of a "saddle-node on an invariant circle" bifurcation: as k_1 decreases through k_1^{SNIC}, a stable periodic solution of finite amplitude disappears because its period diverges to infinity, and it is replaced by a pair of steady states, a stable node [the lower solid curve in Fig. 3(b)] and an unstable saddle point (the dashed curve). Following this curve of saddle points, we find that it folds into a different curve of nodes at $k_1^{SN} = 0.0029864$.

Examining the upper branch of steady-state solutions in Fig. 3(b), we find two additional Hopf bifurcations at $k_1^{H'} = 0.0029870$ and $k_1^{H''} = 0.0041859$. Between these limits the stable steady state coexists (in part) with unstable limit cycles. The larger branch of unstable limit cycles

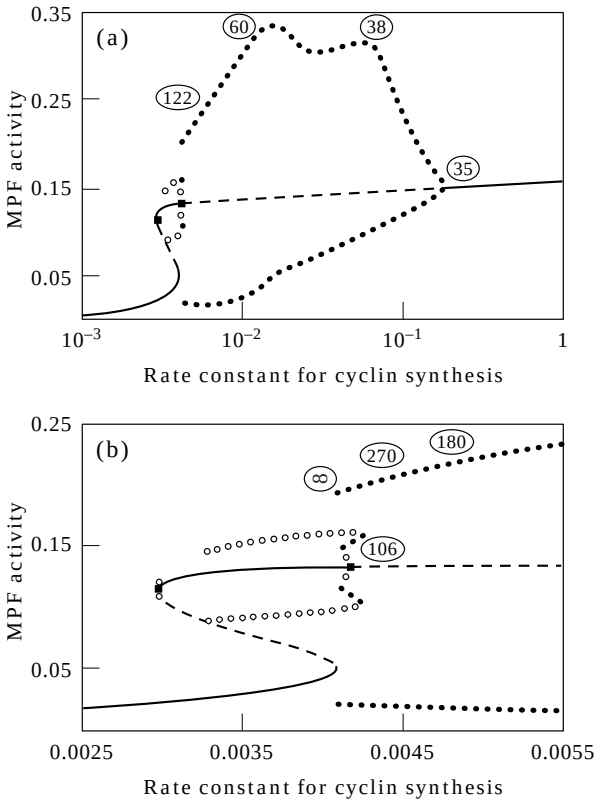

FIG. 3. One-parameter bifurcation diagram. Rate constant for cyclin synthesis = k_1. (—— stable steady state, (– – –) unstable steady state, (●) stable limit cycle, (○) unstable limit cycle, (■) Hopf bifurcation points. For each limit cycle, the upper (lower) circle represents the maximum (minimum) value of MPF observed during an oscillation. To interpret this diagram, you must think of k_1 fixed at a certain value and MPF activity varying periodically with time between the two limits on the figure. The encircled numbers indicate the period of oscillation at different values of k_1. In (a), notice the logarithmic scale for k_1; (b) is a blow-up of the region of multiple stable solutions.

derives from a subcritical Hopf bifurcation at $k_1^{H''}$ and disappears at a saddle-loop bifurcation at $k_1^{SL} = 0.0032912$. The tiny branch of unstable limit cycles bifurcates from the subcritical Hopf bifurcation at $k_1^{H'}$ and disappears almost immediately at a saddle-loop bifurcation.

3. Experimental Predictions

As we have pointed out, the rate of cyclin synthesis (k_1) can be controlled experimentally in frog egg extracts by enzymatic degradation of endogenous mRNAs and then addition of exogenously synthesized cyclin mRNA (Murray & Kirschner, 1989). The one-parameter bifurcation diagram described in Fig. 3 makes some remarkable predictions about the behavior of a sequence of extracts prepared with increasing amounts of cyclin mRNA. Let $k_1 = 0.015$ represent the standard rate of cyclin synthesis in oscillating extracts (period ≈ 60 min). At a 20-fold higher rate ($k_1 = 0.3$), the extract should arrest in a mitotic state, with high MPF activity; and at a 10-fold lower rate ($k_1 = 0.0015$), the extract should arrest in interphase with low MPF activity. By setting up a series of mRNA-ablated egg extracts supplemented with increasing amounts of exogenous cyclin mRNA, one could search for the bifurcation points that separate these qualitatively distinct behaviors.

These bifurcation points will have distinct and easily recognized properties, according to Fig. 3. At high levels of cyclin mRNA, one should observe a supercritical Hopf bifurcation. Just below the bifurcation point, extracts would exhibit MPF oscillations of small amplitude (perhaps MPF activity does not drop low enough for nuclei to go into interphase). The period of these oscillations should be short (≈ 35 min) and show little dependence on mRNA level. In addition, maximum MPF activity in this series of extracts increases dramatically as cyclin mRNA level decreases! This prediction is surprising because one would expect that less cyclin mRNA would generate less cyclin protein and, consequently, less MPF activity. However, because of subtle interactions between MPF and APC, a slower rate of cyclin synthesis reduces the extent of APC activation and permits a larger amplitude of MPF oscillations.

At low mRNA levels, the model predicts a SNIC bifurcation: the oscillatory solution has large amplitude (i.e. it drives nuclei in and out of mitosis), and the period becomes very long as the level of cyclin mRNA approaches the bifurcation point [Fig. 3(b)]. Just below the bifurcation point, the extract will arrest in interphase, with low MPF activity. Notice, however, that just below the SNIC bifurcation (for k_1 between 0.0029864 and 0.0040975) the model exhibits *two* steady states, with low and high MPF activities, respectively. It would be striking to confirm this feature of the model experimentally, but our calculations (not shown) indicate that the domain of attraction of the stable metaphase-arrested steady state is too small to be found by simple perturbations (e.g. by adding active MPF to the interphase-arrested extract).

In Fig. 3(b) there is a tiny region, $0.0041282 < k_1 < 0.0042567$, where two stable oscillatory solutions coexist. Although it would be impossible to confirm this prediction experimentally, it illustrates the complexity of behavior possible in this control system.

4. Two-parameter Bifurcation Diagrams

Are the predictions made on the basis of Fig. 3 reliable when we acknowledge that the parameter values estimated by Novak & Tyson (1993a) are quite uncertain? What becomes of our one-parameter bifurcation diagram if we start to vary a second, third, fourth parameter? Are the predictions robust? Do they hold up in the face of uncertainty about the other parameters in the model?

We approach this question by characterizing the bifurcation diagram of the model when two parameters are varied simultaneously. First we will construct a two-parameter bifurcation diagram based on k_1 and $V_{2''}$ (the rate constant for cyclin degradation when the APC is active). This diagram gives a planar section through the full 26-dimensional parameter space. Then we will examine two other planar sections: (1) k_1 and $[Wee1]_{total}$ (the total amount of Wee1 in the extract), and (2) k_1 and $[Cdc25]_{total}$. We will show that all two-parameter bifurcation diagrams

have certain generic features that are subject to experimental verification.

A two-parameter bifurcation diagram is constructed as follows. Let us start in Fig. 3(a) at the SN bifuration at $k_1 = 0.0029864$. We ask AUTO to do the following: change k_1 a little bit (the system moves off the point of SN bifurcation), then change $V_{2''}$ just enough to bring the system back to a SN bifurcation point. By repeating this process many times, AUTO can trace out a locus of SN bifurcation points in the (k_1, $V_{2''}$) parameter plane [the red, inverted **V** in Fig. 4(a)]. We see that there are two loci of SN bifurcations, which come together at a cusp point. The left-hand branch contains the SN bifurcation at $k_1 = 0.0029864$ in Fig. 3(a), and the right-hand branch contains the SN fold which is a component of the SNIC bifurcation at $k_1 = 0.0040975$ in Fig. 3(a). Inside the **V**, the system exhibits three steady states (two nodes and a saddle point). Outside the **V**, the system has only one steady-state solution.

Each branch of the **V** is a locus of "codimension-one" bifurcation points, because we need vary only one parameter (either k_1 or $V_{2''}$) to cross the bifurcation. The cusp is a "codimension-two" bifurcation point, because we must specify the values of two parameters (both k_1 and $V_{2''}$) in order to locate this point. Bifurcation theory tells us that the **V**-shape of these SN bifurcations is "generic", i.e. it is not a freakish property of our specific choice of parameters, but rather **V**-shaped loci of SN bifurcations can be expected in any planar section through parameter space.

Next, we return to the Hopf bifurcation at $k_1 = 0.18226$ in Fig. 3(a), and we ask AUTO to follow it. AUTO returns with a closed curve [blue in Fig. 4(a)] of Hopf bifurcation points. Inside this closed curve we always find an unstable steady state accompanied by a stable periodic solution; outside, the steady state is stable. It should be obvious that the Hopf bifurcations at 0.18226 and 0.0041859 in Fig. 3 belong to the blue curve in Fig. 4(a), but the Hopf bifurcation at 0.0029870 in Fig. 3(b) does not. Asking AUTO to follow the latter point, we get the light blue curve of Hopf bifurcations in Fig. 4(b), which seems to attach in two places to the red curve of SN bifurcations. Consulting any standard text on bifurcation theory, we find that such attachment points are typical of a codimension-two bifurcation first described by Takens & Bogdanov (TB). At a TB bifurcation there must also exist a third locus of codimension-one bifurcation points, called saddle-loop (SL) bifurcations [the green curves in Fig. 4(b)]. At an SL bifurcation, a limit cycle is annihilated by a saddle point; consequently the period of oscillation diverges ($\rightarrow \infty$) at the bifurcation point. The SL loci emanating from the TB bifurcation points attach elsewhere to the SN curve at two SNL points (saddle-node-loop bifurcations, codimension two). Between the two SNLs, we have a locus of codimension-one SNIC bifurcations.

The basic structure of Fig. 4 is familiar to experts in chemical dynamics. The cusp-shaped region of multiple steady states with a loop of Hopf bifurcations attached at two TBs is a

FIG. 4. Two-parameter bifurcation diagram (incomplete). Rate constant for cyclin degradation = $V_{2''}$. Dashed horizontal line at $V_{2''} = 1$ represents the one-parameter cut in Fig. 3. (a) Within the red **V**-shaped region, bounded by saddle-node (SN) bifurcations, there exist three steady-state solutions; outside only one. Within the closed blue curve of Hopf (H) bifurcations, there exist an unstable steady state and a stable limit cycle; (b) a second locus of Hopf bifurcations (light blue) attaches to the SN loci (red) at two Takens–Bogdanov bifurcation points (TB), along with a locus of saddle-loop (SL) bifurcations (green). The SL loci also attach to SN loci at two saddle-node-loop bifurcation points (SNL). Between the SNLs the bifurcation curve is a SNIC (saddle-node on an invariant circle).

FIG. 5. Two-parameter bifurcation diagram (complete). Key: red = saddle-node (SN), blue = Hopf (H), green = saddle-loop (SL), black = cyclic fold (CF). The phase portraits in each region of parameter space are described by icons: s = stable node, u = unstable node, x = saddle point, solid circle = stable limit cycle, dashed circle = unstable limit cycle.

FIG. 7. Stable limit cycle oscillations: (a) the thick colored curves follow limit cycles of fixed period (20 min, 25 min, etc.) across the two-parameter plane; (b) the region of existence of at least one stable limit cycle is delineated by pieces of various bifurcation sets that compose the outer edge of this bounded domain. Within the domain there are several subdomains with at least one other stable solution.

generic feature of reaction mechanisms with positive feedback loops (autocatalysis) (Guckenheimer, 1986), and the closed loop of Hopf bifurcations (dark blue) is typical of negative feedback oscillators (Goldbeter & Guilmot, 1996).

The two-parameter bifurcation diagram (Fig. 4) is incomplete because we have yet to account for places where periodic solutions change their stability. Hopf bifurcations change from subcritical to supercritical at codimension-two, degenerate Hopf (DH) bifurcation points; and saddle-loops change from stable to unstable at codimension-two, neutral saddle-loop (NSL) bifurcation points. For our model, AUTO finds six DH points and two NSL points. At each of these eight codimension-two bifurcation points there appears a branch of cyclic fold (CF) bifurcations: codimension-one bifurcations where stable and unstable limit cycles coalesce and disappear. There are four CF branches that connect the DH and NSL points in pairs: DH_1 to NSL_2, DH_2 to DH_5, DH_3 to DH_4, and DH_6 to NSL_1 (see Figs 5 and 6).

This completes our description of the two-parameter bifurcation diagram for the Novak–Tyson model, using the parameter set in their 1993 paper. Full details of the diagram are given in Figs 5 and 6, along with icons that present all the qualitatively different phase portraits predicted by the model.

5. Biological Implications

Figure 5 gives a comprehensive view of the different types of behavior implicit in the relatively simple molecular network controlling MPF activity in frog egg extracts. We can think of all the "action" occurring in a restricted domain of parameter space. On the outskirts of this domain, the control system is arrested at a unique stable steady state. Within the domain, the system exhibits stable oscillatory solutions, multiple steady states, and bi-rythmicity (coexisting stable limit cycles). The largest subdomain, bounded in part by the dark blue Hopf curve in Fig. 5, has a simple phase portrait: a single unstable steady state accompanied by a stable limit cycle, with period 20–60 min. This subdomain corresponds to the well-known oscillatory behavior of Murray–Kirschner (Murray & Kirschner, 1989) cycling extracts. It is reassuring to notice that this behavior is very robust: the oscillations persist over a broad range of rates of cyclin synthesis and degradation. As we shall show later, these oscillations are crucially dependent on the negative feedback loop of MPF on its own destruction, through IE and APC [Fig. 2(c)].

A second subdomain of simple oscillations (stable limit cycle and a single unstable steady state) exists at large values of $V_{2'}$ (bounded by the light blue curve in Fig. 5). These oscillations are diven by the positive feedback loops: MPF activates its friend (Cdc25) and inhibits its enemy (Wee1).

Stable limit cycle solutions exist only within a restricted region of the two-parameter plane. Figure 7(a) shows how the period of oscillation depends on position within this region. Figure 7(b) shows that the oscillatory domain is bounded by bits and pieces of the bifurcation sets in Fig. 5, and delineates subdomains where other stable solutions coexist with a stable limit cycle. Figure 7(b) demonstrates that the tiny slice of bi-rhythmicity in Fig. 3 opens up into a larger stretch of k_1 values at larger values of $V_{2'}$. There is even a tiny region of tri-stability in parameter space. Although it would be difficult to confirm these regions of multi-stability, we should remember that the MPF regulatory system has the potential for such complex behavior.

As we get into the region of multiple steady states, within the red cusp in Fig. 5, the behavior of the control system becomes very complicated indeed. This complexity of solutions is not a freakish property of the Novak–Tyson model; rather it is exactly what can be expected of a dynamical system that admits both limit cycle oscillations and multiple steady states. Where the two types of solutions collide, they typically generate this sort of hodge-podge of solutions (Guckenheimer, 1986).

Might the complex dynamical properties of the MPF regulatory system play important roles in control of the cell cycle? It is too early to answer this question. There is no experimental

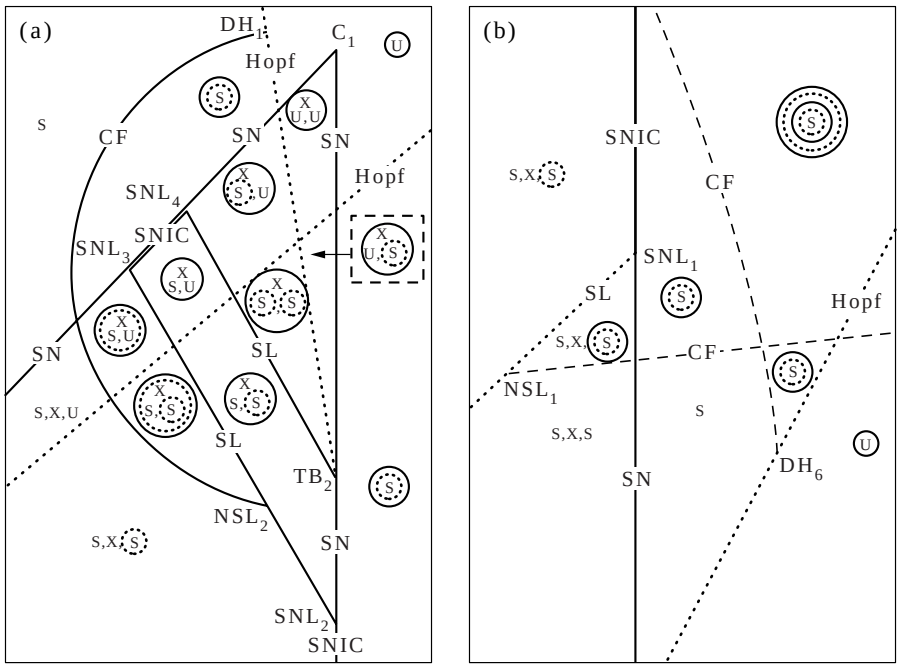

FIG. 6. Schematic representations of the most complicated regions of the two-parameter bifurcation diagram.

evidence for any behavior subtler than a stable steady state (cell cycle arrest) or a simple oscillation (mitotic cycles in early embryos). On the other hand, no one has ever thought to look for evidence of these more complex phase portraits in the physiology and biochemistry of the eukaryotic cell division cycle.

6. How Robust are these Results?

6.1. TO CHANGES IN GENE DOSAGE

Many rate constants are proportional to total enzyme concentration and thus may vary by two-fold between homozygous and heterozygous individuals, if the heterozygote carries a non-functional copy of the gene. In general we would expect a two-fold change in parameter value to cause a significant change in the period of a limit cycle oscillation, and it might eliminate the limit cycle altogether (by driving the system across a bifurcation set). However, our model of MPF oscillations has the unexpected virtue that the period of the limit cycle is quite insensitive to the total concentration of key regulatory enzymes, over a broad range of concentrations (see Fig. 8).

6.2. TO MAJOR RE-ADJUSTMENTS OF THE PARAMETER SET

Recently, Marlovits *et al*. (1998) have re-estimated the parameters of the Novak–Tyson model (Table 2), based on careful kinetic measurements by Kumagai & Dunphy (1995). Figure 9(a) shows that this presumably better set of rate constants predicts a two-parameter bifurcation diagram very similar to Fig. 5,

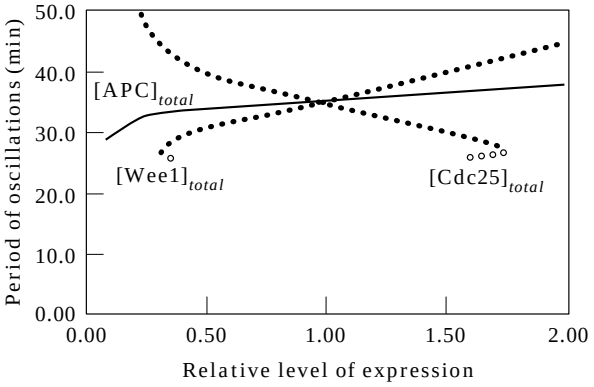

FIG. 8. Period of oscillation as a function of the amounts of the major regulatory enzymes. The parameter set in Table 2 is normalized so that $[Wee1]_{total} = [Cdc25]_{total} = [APC]_{total} = 1$. If we were to change the level of expression of one of these genes, then the total protein concentration would deviate from 1. This figure demonstrates that the period of limit cycle oscillations is quite insensitive to expression level over at least a four-fold range.

Fig. 4

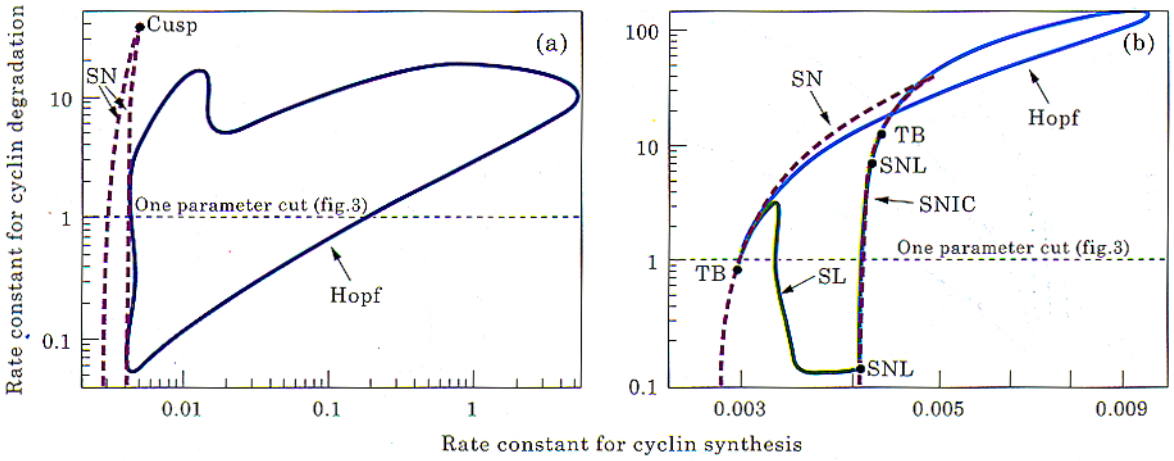

Fig. 5

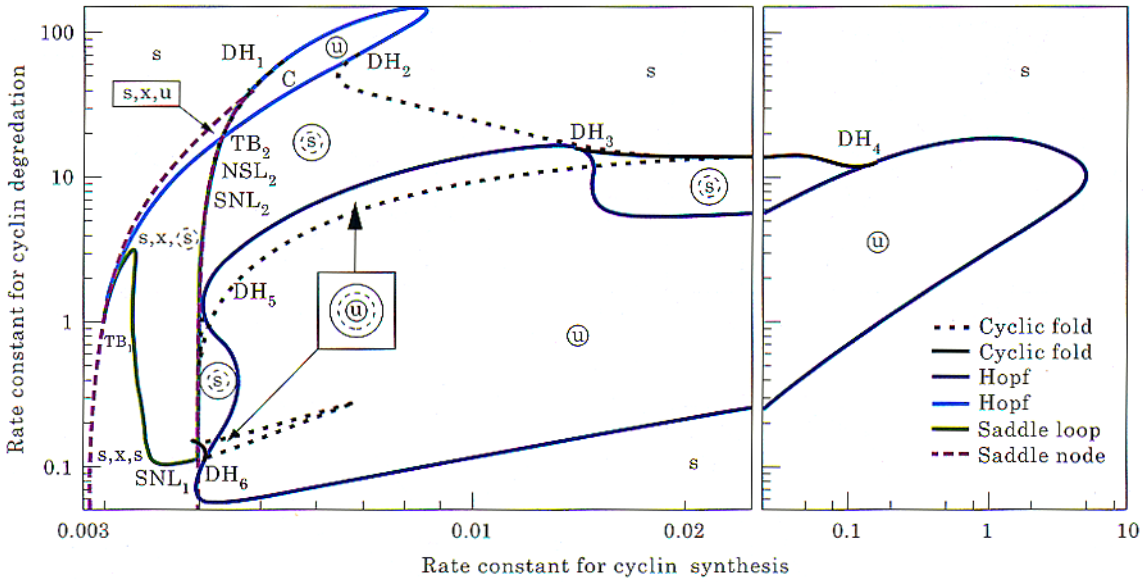

Fig. 7

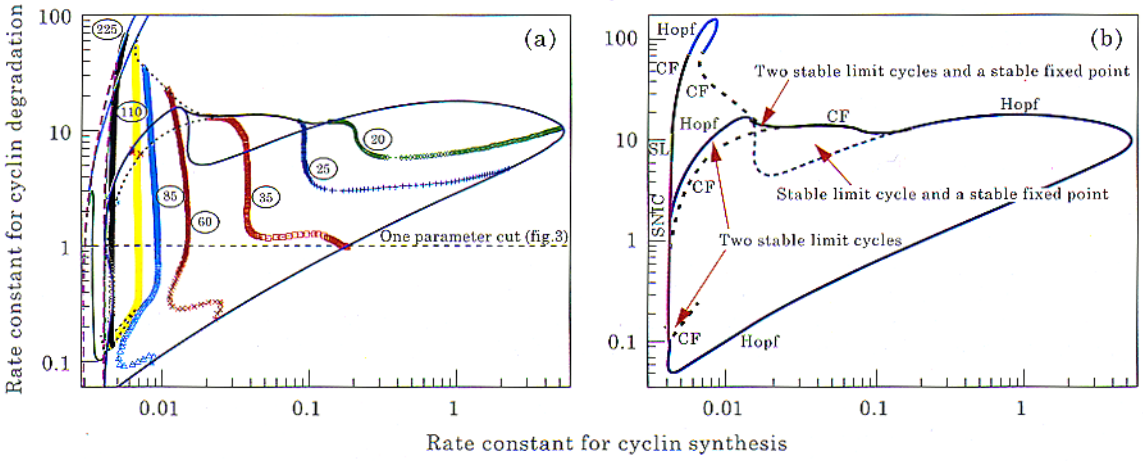

computed for the original parameter set. This observation suggests that the basic features of the two-parameter bifurcation diagram are not sensitive to precise values of the other parameters in the model.

6.3. TO DIFFERENT PLANAR CUTS THROUGH PARAMETER SPACE

Figure 9(a) shows one planar slice through a 26-dimensional parameter space. Are the strange features of this diagram unique to how we have sliced the object? In Fig. 9(b,c) we show two additional slices: k_1 vs. $[Wee1]_{total}$ and k_1 vs. $[Cdc25]_{total}$. Although these slices look quite different from each other and from the k_1 vs. $V_{2'}$ slice, they are all composed of the same generic elements: a **V**-shaped domain of multiple steady states, two families of Hopf bifurcations, and a long stretch of SNIC bifurations (where the red and green curves overlap). Loosely speaking, the universe of different types of behavior in 26-dimensional parameter space looks equally strange no matter how you slice it!

6.4. TO CHANGES IN THE UNDERLYING MODEL

Finally, we can use AUTO to determine to what degree the full Novak–Tyson model (with nine variables) can be reduced without losing vital qualitative features of the solution set. In an earlier paper, Novak & Tyson (1993b) used singular perturbation theory to simplify their model to just two DEs: for active MPF and total cyclin. Although the two-component version still shows oscillations and arrested states, it does not have the wealth of complex bifurcations observed in the nine-component model [see Fig. 10(a)]. The two-component model has a **V**-shaped region containing multiple steady states, and a loop of Hopf bifurcations connected to the **V** at TB points, but it lacks the large region of oscillatory solutions enclosed by the dark blue curve of Hopf bifurcations in Fig. 4.

Following the lead of that paper, we have simplified the model in stages and recomputed the two-parameter bifurcation diagram to see how the behavior of the model depends on its complexity. If we let $k_3 \to \infty$ (fast dimerization of Cdc2 and cyclin) and $k_{CAK} \to \infty$ (fast phosphorylation of threonine-161), we simplify the system from nine variables to six, because we can eliminate cyclin monomers and express the concentrations of T161 unphosphorylated dimers in terms of T161 phosphorylated dimers. Nonetheless, there are no significant changes in the two-parameter bifurcation diagram [see Fig. 10(b)]. In addition, we can assume rapid phosphorylation and dephosphorylation of Wee1 or Cdc25, reducing the model from six variables to four, and still retain all the characteristic features of the two-parameter bifurcation diagram [Fig. 10(c)]. However, if we assume rapid phosphorylation and dephosphorylation of IE, the model loses the large region of limit cycle oscillations and the diagram looks like Fig. 10(a). Since the role of IE is to introduce a time delay in the activation of APC by MPF, we conclude that the region of oscillations within the dark blue curve in Fig. 4 is attributable to the negative feedback loop in the model. Oscillations within the light blue loop, on the other hand, are generated by the positive feedback loops, whereby MPF activates Cdc25 and inhibits Wee1.

7. Discussion

Using bifurcation theory, we have uncovered an unexpectedly complex collection of physiologically distinct behaviors exhibited by the biochemical network that controls MPF activity in frog eggs. Some solutions of the model equations correspond to well-known physiological states of the egg: interphase arrest with low MPF activity (immature oocyte), M-phase arrest with high MPF activity (mature egg), and spontaneous limit cycle oscillations (autonomous mitotic cycles of the early embryo) (Tyson, 1991). Other sets of solution are more bizarre and have never been recognized experimentally: for example, coexisting states of interphase and M-phase arrest, or two stable oscillatory solutions of different amplitude and period.

7.1. EXPERIMENTAL TESTS

Our theoretical analysis of the MPF control system makes some dramatic predictions about where to look for unusual behavior. The basic

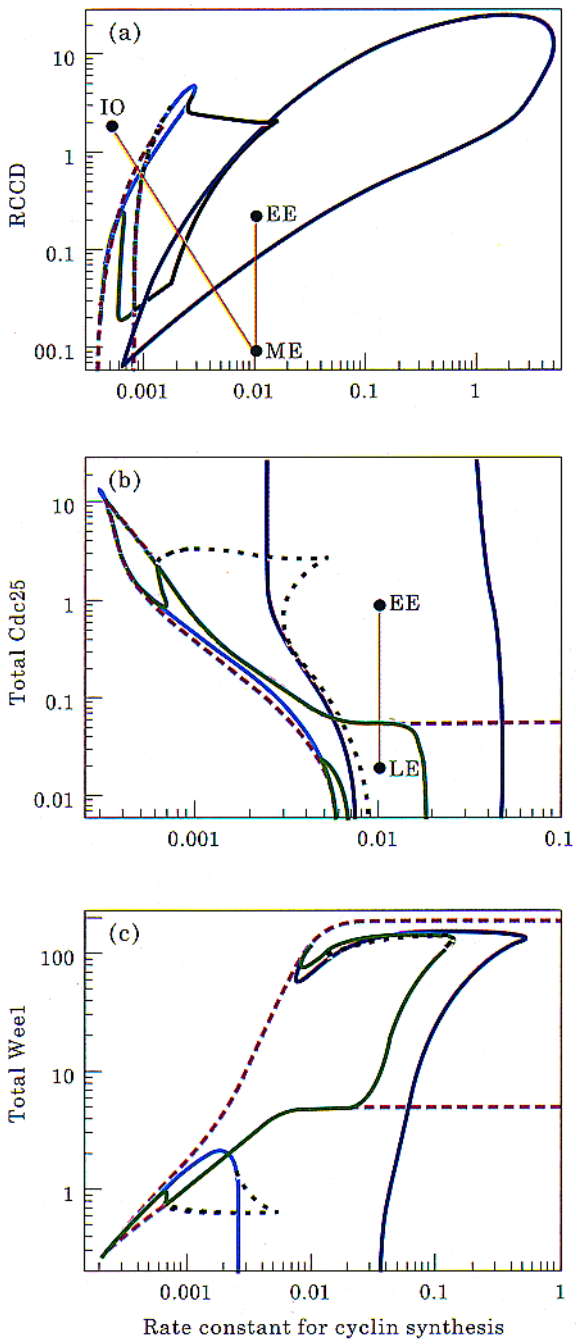

Fig. 9

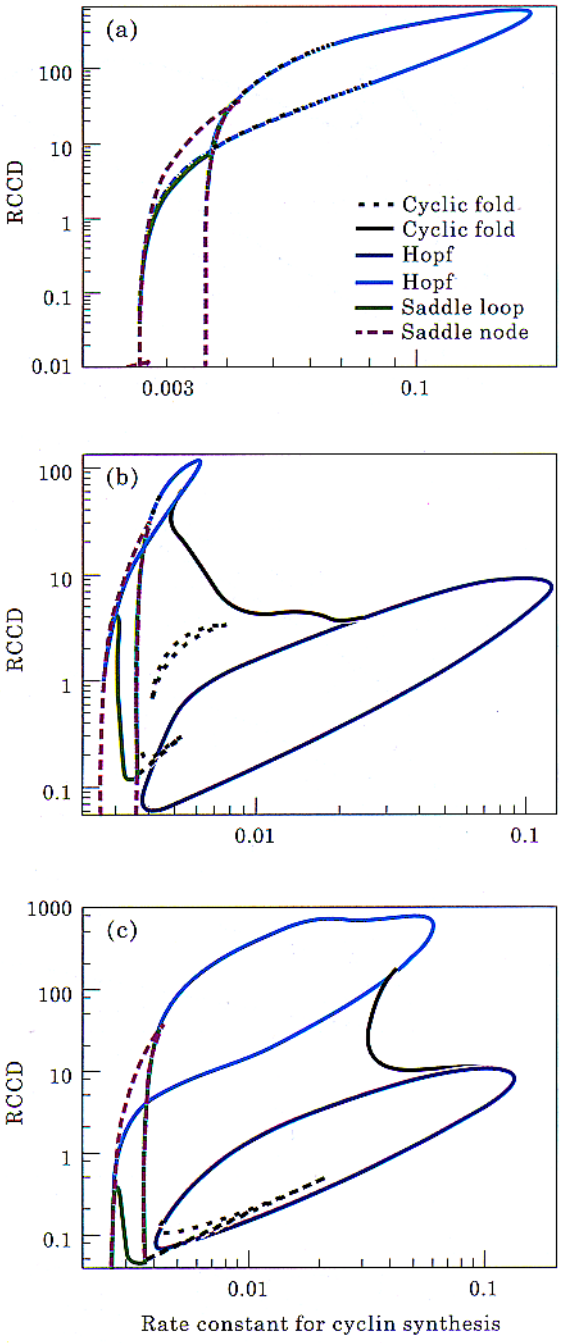

Fig. 10

FIG. 9. Two-parameter bifurcation diagrams for the 1998 parameter set: (a) all the major conclusions we have drawn from Fig. 5 (the corresponding diagram for the 1993 parameter set) are still valid; (b) and (c) bifurcation diagrams using $[Cdc25]_{total}$ and $[Wee1]_{total}$ as the second parameter. We use the same color scheme as before (Figs 4 and 5) for the bifurcation curves. Developmental paths: IO = immature oocyte, ME = mature egg, EE = early embryo, LE = late embryo.

FIG. 10. Bifurcation diagrams for reduced versions of the Novak–Tyson model. Basal parameters: 1993 set. RCCD = rate constant for cyclin degradation: (a) the two-variable model [active MPF and total cyclin only; see Novak & Tyson (1993a)]; (b) six-variable model (active MPF, total cyclin, Wee1, Cdc25, IE, APC); (c) four-variable model (active MPF, total cyclin, IE, APC).

protocol calls for *Xenopus* egg extracts depleted of maternal mRNA and supplemented with controlled quantities of cyclin B mRNA (Murray & Kirschner, 1989).

1. At low levels of cyclin mRNA, extracts should arrest in interphase, at intermediate levels they should exhibit mitotic oscillations, and at high levels they should arrest in M phase.

2. As cyclin mRNA level is adjusted carefully between these three regimes, the extracts should undergo characteristic transitions (bifurcations). As mRNA content is reduced from high levels, the mitotic-arrested state should lose stability by a Hopf bifurcation, meaning that MPF oscillations, at first, have small amplitude. MPF activity might not fluctuate enough to drive sperm nuclei in and out of mitosis (the easy way to assay MPF fluctuations in extracts), but oscillations could be detected by histone H1 kinase assays. As cyclin mRNA level is reduced further, the model predicts that maximum cyclin protein content (and MPF activity) in the extract would increase abruptly, but the period of oscillation would increase only slightly: both of these predictions are counterintuitive. At still lower levels, the period of oscillation would abruptly lengthen, and the extract would arrest in interphase, with plenty of cyclin and low MPF activity. The model predicts that, at high levels of cyclin mRNA, the oscillatory state should be lost as the amplitude of oscillation goes to zero with the period of oscillation holding constant, a signature of Hopf bifurcation. On the other hand, at low levels of cyclin mRNA, oscillations should be lost as the period goes to infinity with the amplitude holding constant, a characteristic of SNIC bifurcation.

3. For cyclin mRNA levels just below the SNIC bifurcation, the extract should exhibit bistable behavior. Sperm nuclei in the extract could arrest either in interphase or in metaphase, depending on subtle details of how the extract is prepared.

4. Also in the vicinity of the SNIC bifurcation, we might find more exotic bistable behavior, e.g. stable MPF oscillations coexisting with a stable arrested state.

In designing such tests, it would be advisable to have experimental control over a second parameter in the model, in order to exploit information in two-parameter bifurcation diagrams. Figure 9 should be especially useful in this regard, because $[Wee1]_{total}$ and $[Cdc25]_{total}$ are parameters that can be manipulated experimentally.

7.2. DEVELOPMENTAL PATHS

Tyson (1991) pointed out that frog eggs seem to use the bifurcation properties of the MPF control system to control cell division during development. By regulating the expression of genes for cyclin B, Wee1 and Cdc25, as well as other genes that interact with the MPF network, the egg can select different regions of parameter space with different physiological properties. For instance, it is well known that, after exposure to progesterone, frog eggs synthesize the *mos* protein, which then interferes with cyclin degradation (Sagata *et al*., 1989; Hunt, 1989). In Fig. 9(a) we show that a large decrease in the rate constant for cyclin degradation, combined with a modest increase in the rate constant for cyclin synthesis, can move an egg from an interphase-arrested steady state to a metaphase-arrested steady state ("developmental path" IO → ME). The fertilized egg must then move across the Hopf bifurcation into the region of sustained oscillations [ME → EE in Fig. 9(a)], which might be attributable to the degradation of Mos after fertilization (Watanabe *et al*., 1989).

As the embryo approaches the mid-blastula transition, cell cycle time lengthens and cells finally arrest in interphase. In *Drosophila* this transition is thought to occur by depleting the egg of Cdc25 (Edgar & O'Farrell, 1990), which suggests that the control system crosses the SNIC bifurcation as indicated in Fig. 9(b) (EE → LE). Cells in this state (LE) are arrested at an interphase checkpoint. In order to enter mitosis, the checkpoint must be lifted; for example, by crossing the SNIC curve into the oscillatory domain (by increasing $[Cdc25]_{total}$) and then returning to the region of interphase arrest (by decreasing $[Cdc25]_{total}$). In this way, cell division can be suited to the differentiation of various tissues in the developing embryo.

In frog eggs, the mid-blastula transition is associated not with fluctuations in Cdc25 level but with a dramatic disappearance of cyclin E

(Hartley *et al*., 1996). Guadagno & Newport (1996) showed that, when Cdk2/cyclin E is blocked by a specific inhibitor, mitotic cycling of frog embryos halts and Cdc2/cyclin B accumulates in the inactive, tyrosine-phosphorylated form, apparently because Cdk2/cyclin E is necessary to keep Cdc25 partially phosphorylated and activated. Therefore, loss of Cdk2/cyclin E activity at the mid-blastula transition might decrease the maximal activity of Cdc25 (changing the parameter $V_{25''}$ in our equations) and thereby create an interphase-arrested state. Release from this checkpoint in later cell cycle may be driven by re-expression of cyclin E or by fluctuations in other cyclin-dependent kinases.

In any case, if embryonic cell cycles are controlled by limit cycles (early) and checkpoints (later), then embryos must adopt parameter values close to all the ''action'' in our bifurcation diagrams, because it is in this region that changes in gene expression can create dramatic changes in cell division. If so, then it will be hard for cells to avoid the more complex bifurcations that come with the territory. Perhaps cells make large changes in parameter values (as in the developmental paths in Fig. 9) so that they skip from one large region of parameter space to another (where the behavior is simple and robust) and thereby miss the smaller domains where complicated bifurcations occur. Although this scenario seems likely to us, we recognize the possibility that cells exploit some of the more complicated bifurcations for subtle physiological purposes. We can cite no examples, but that may say more about what physiologists recognize and name than what frog eggs are capable of doing.

Pancreatic cells are known to generate complex ''bursting'' patterns of insulin secretion that depend on crossing bifurcation sets similar to the ones we have discovered here (Sherman, 1997). We propose that cell cycle regulation, like plasma glucose regulation, is intimately tied to bifurcations in the dynamics of the underlying molecular mechanism. In this paper we have shown what complexity is inherent to the MPF control system. Later in development, at least four different kinase/cyclin pairs and their ancillary proteins govern the full cell cycle of vertebrates. To understand the bifurcation properties of such comprehensive mechanisms and the role they play in the physiology of the cell cycle will be a major challenge for future modeling in this field.

7.3. CHECKPOINTS

The current paradigm of cell cycle control in eukaryotes posits a linear sequence of three checkpoints: at the G1/S transition, the G2/M transition, and the meta/anaphase transition (Alberts *et al*., 1994). Cells progress through the division cycle, according to this view, by transiting from one checkpoint to the next. Before they may pass the G1 checkpoint and enter S phase, cells must grow large enough to warrant a new round of DNA synthesis and they must acquire the proper ''visas''. (For example, mammalian cells generally require exposure to circulating growth factors, whereas budding yeast cells require that sex pheromones be absent from their external environment). Before passing the G2 checkpoint and entering mitosis, cells make sure that their DNA is completely and correctly replicated, and before separating sister chromatids at anaphase, cells make sure that every chromosome is properly aligned on the mitotic spindle.

We contend that these checkpoints are stable, steady-state solutions of the underlying kinetic equations governing cell cycle events. In this view, checkpoints are imposed/lifted by bifurcations that create/destroy stable steady states. In this paper we have illustrated several kinds of bifurcations that could serve this role. For instance, a checkpoint could be lifted at a Hopf bifurcation, where a steady state loses stability, or at a saddle-node bifurcation, where a stable steady state is annihilated by coalescing with an unstable saddle point. Both scenarios have been proposed to explain cell cycle transitions in eukaryotes (Tyson, 1991; Novak & Tyson, 1993a, 1997; Thron, 1997), and SNIC bifurcations work equally well (Kaern & Hunding, 1998). The best experimental system for testing these theoretical ideas is the frog egg extract. If we can show (as proposed above) that mitotic cycles are lost at low levels of cyclin mRNA by a SNIC or SL bifurcation (infinite period), we will have direct evidence that cell cycle transitions are intimately tied to subtle bifurcation processes.

7.4. MUST THE FROG-EGG MODEL BE SO COMPLICATED?

In analysing a model of time-delayed negative feedback in cyclin degradation (without positive feedback of MPF on Wee1 and Cdc25), Goldbeter & Guilmot (1996) found robust oscillations but no evidence of multiple steady states. Our analysis of the Novak–Tyson model shows that the negative feedback loop does indeed play an essential role in generating robust MPF oscillations characteristic of frog egg extracts and embryos. If we remove the time delay from the negative feedback loop (by assuming that IE responds rapidly to changes in MPF activity), then we lose the large domain of robust oscillations bounded by the dark blue curve in Fig. 10(c). The only remaining oscillatory domain relies on the positive feedback loop generating large fluctuations in tyrosine-15 phosphorylation, which are not observed in mitotic oscillations in intact embryos (Ferrell *et al*., 1991).

The essential features of mitotic control in *Xenopus* (multiple steady states and robust oscillations) seem to depend on both the positive and negative feedback loops known to exist in the MPF regulatory system. We cannot adequately describe the behavior of frog egg cell cycles with simplified models, like those initially proposed by Goldbeter (1991), Norel & Agur (1991), Tyson (1991). Although these simple models may be useful in understanding certain features of mitotic control, they do not tell the whole story. Therefore we must have tools for studying the dynamics of large sets of coupled DEs that govern realistic reaction mechanisms with many interacting components. We have found that a combination of computational and analytical tools works well. Singular-perturbation arguments can be used to simplify complex models, so that the intuitively appealing, geometrical tools of phase plane analysis can be applied to subsets of the full network. Then accurate numerical solutions of the DEs can be computed, to support the predictions of simplified models and to provide quantitative data for comparison to experiments. Finally, the theory of codimension-one and -two bifurcation sets, in combination with powerful numerical programs like AUTO, can be used to unravel the properties of complex networks with many interacting components.

Kathy Chen helped us considerably in preparing this material for an audience of cell and molecular biologists. Garry Odell gave us many valuable suggestions about applying our analysis to frog egg extracts. John Guckenheimer advised us in the early stages of pinning down Fig. 5. This work was supported by National Science Foundation Grants MCB-9600536 and DBI-9724085.

REFERENCES

Alberts, B., Bray, D., Lewis, J., Raff, M., Roberts, K. & Watson, J. D. (1994). *Molecular Biology of the Cell*, 3rd Edn, Chap. 17. New York: Garland Publishing.

Borisuk, M. T. (1997). Bifurcation analysis of a model of the frog egg cell cycle. Ph.D. Thesis. Virginia Polytechnic Institute & State University, Blacksburg, VA. http://scholar.lib.vt.edutheses/etd-search.html

Doedel, E. J. & Wang, X. J. (1995). AUTO94: software for continuation and bifurcation problems in ordinary differential equations. Pasadena, CA: Center for Research on Parallel Computing, California Institute of Technology.

Edelstein-Keshet, L. (1988). *Mathematical Models in Biology*. New York: Random House.

Edgar, B. A. & O'Farrell, P. H. (1990). The three postblastoderm cell cycles of *Drosophila* embryogenesis are regulated in G2 by *string*. *Cell* **62,** 469–480.

Ferrell, Jr., J. E., Wu, M., Gerhart, J. C. & Martin, G. S. (1991). Cell cycle tyrosine phosphorylation of $p34^{cdc2}$ and a microtubule-associated protein kinase homolog in *Xenopus* oocytes and eggs. *Mol. Cell. Biol.* **11,** 1965–1971.

Goldbeter, A. (1991). A minimal cascade model for the mitotic oscillator involving cyclin and cdc2 kinase. *Proc. Nat. Acad. Sci. U.S.A.* **88,** 9107–9111.

Goldbeter, A. & Guilmot, J. M. (1996). Thresholds and oscillations in enzymatic cascades. *J. Phys. Chem.* **100,** 19174–19181.

Guadagno, T. M. & Newport, J. W. (1996). Cdk2 kinase is required for entry into mitosis as a positive regulator of Cdc2-cyclin B kinase activity. *Cell* **84,** 73–82.

Guckenheimer, J. (1986). Multiple bifurcation problems for chemical reactors. *Physica* **20D,** 1–20.

Hartley, R. S., Rempel, R. E. & Maller, J. L. (1996). *In vivo* regulation of the early embryonic cell cycle in *Xenopus*. *Devel. Biol.* **173,** 408–419.

Hunt, T. (1989). Under arrest in the cell cycle. *Nature* **342,** 483–484.

Kaern, M. & Hunding, A. (1998). Dynamics of the cell cycle engine: Cdc2-kinase and the transition into mitosis. *J. theor. Biol.* **193,** 47–57.

Kaplan, D. & Glass, L. (1995). *Understanding Nonlinear Dynamics* Chap. 5. New York: Springer-Verlag.

Kumagai, A. & Dunphy, W. G. (1995). Control of the Cdc2/Cyclin B complex in *Xenopus* egg extracts arrested at a G2/M checkpoint with DNA synthesis inhibitors. *Mol. Biol. Cell* **6,** 199–213.

KUZNETSOV, Y. A. (1995). *Elements of Applied Bifurcation Theory*. New York: Springer-Verlag.

LODISH, H., BALTIMORE, D., BERK, A., ZIPURSKY, S. L., MATSUDAIRA, P. & DARNELL, J. (1995). *Molecular Cell Biology*, 3rd Edn, Chap. 25. New York: W. H. Freeman Co.

MARLOVITS, G., TYSON, C. J., NOVAK, B. & TYSON, J. J. (1998). Modeling M-phase control in *Xenopus* oocyte extracts: the surveillance mechanism for unreplicated DNA. *Biophys. Chem*., **72,** 169–184.

MURRAY, A. & HUNT, T. (1993). *The Cell Cycle. An Introduction*. New York: W. H. Freeman Co.

MURRAY, A. W. & KIRSCHNER, M. W. (1989). Cyclin synthesis drives the early embryonic cell cycle. *Nature* **339,** 275–280.

NAYFEH, A. H. & BALACHANDRAN, B. (1985). *Applied Nonlinear Dynamics. Analytical, Computational, and Experimental Methods*. New York: John Wiley & Sons.

NOREL, R. & AGUR, Z. (1991). A model for the adjustment of the mitotic clock by cyclin and MPF levels. *Science* **251,** 1076–1078.

NOVAK, B. & TYSON, J. J. (1993a). Numerical analysis of a comprehensive model of M-phase control in *Xenopus* oocyte extracts and intact embryos. *J. Cell Sci*. **106,** 1153–1168.

NOVAK, B. & TYSON, J. J. (1993b). Modeling the cell division cycle: M-phase trigger, oscillations and size control. *J. theor. Biol*. **165,** 101–134.

NOVAK, B. & TYSON, J. J. (1997). Modeling the control of DNA replication in fission yeast. *Proc. Nat. Acad. Sci. U.S.A*. **94,** 9147–9152.

ODELL, G. M. (1980). Qualitative theory of systems of ordinary differential equations, including phase plane analysis and the use of the Hopf bifurcation theorem. In: *Mathematical Models in Molecular and Cellular Biology*. (Segel, L. A., ed.) pp. 649–727. Cambridge: Cambridge University Press.

SAGATA, N., WATANABE, N., VANDE WOUDE, G. F. & IKAWA, Y. (1989). The *c-mos* proto-oncogene product is a cytostatic factor responsible for meiotic arrest in vertebrate eggs. *Nature* **342,** 512–518.

SEGEL, L. A. (1984). *Modeling Dynamic Phemomena in Molecular and Cellular Biology*. Cambridge: Cambridge University Press.

SHERMAN, A. (1997). Calcium and membrane potential oscillation in pancreatic β cells. In: *Case Studies in Mathematical Modeling: Ecology, Physiology and Cell Biology*. (Othmer, H. G., Adler, F. R., Lewis, M. A. & Dallon, J. C., eds) pp. 199–217. Upper Saddle River, NJ: Prentice Hall.

STROGATZ, S. H. (1994). *Nonlinear Dynamics and Chaos*. Reading, MA: Addison-Wesley.

THRON, C. D. (1997). Bistable biochemical switching and the control of the events of the cell cycle. *Oncogene* **15,** 317–325.

TYSON, J. J. (1991). Modeling the cell division cycle: cdc2 and cyclin interactions. *Proc. Nat. Acad. Sci. U.S.A*. **88,** 7328–7332.

WATANABE, N., VANDE WOUDE, G. F., IKAWA, Y. & SAGATA, N. (1989). Specific proteolysis of the c-*mos* proto-oncogene product by calpain on fertilization of *Xenopus* eggs. *Nature* **342,** 505–511.

APPENDIX

Primer on Bifurcation Theory

Fuller introductions to bifurcation theory can be found in Strogatz (1994), Borisuk (1997). Industrial strength treatises that we consulted are Nayfeh & Balachandran (1985), Guckenheimer (1986), Kuznetsov (1995).

A kinetic model of a biochemical control system, like Fig. 2 and Table 1, consists of differential equations (DEs), one for each time-varying component (“variable”) in the reaction network. The right-hand-side of each DE is a sum of terms, each one representing a reaction in the network. Each term is preceded by a + or − sign depending on whether its reaction increases or decreases the concentration (or relative activity) of the variable. Each

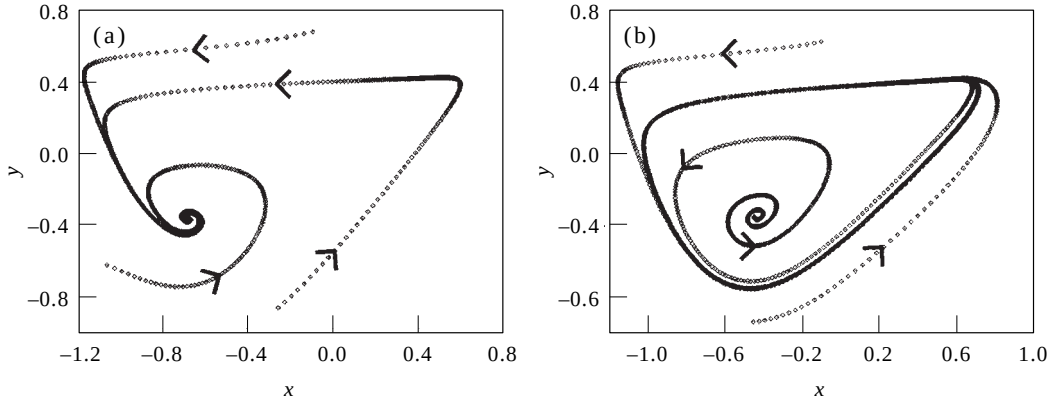

FIG. A1. Phase plane portraits for eqn (*) in the Appendix. Each curve (trajectory) is a locus of points traced out by a solution $x(t)$ and $y(t)$, as t varies from 0 to ∞. Parameter values: $b = 0.5$, $c = 0.1$, $p = 1$: (a) $a = -0.8$; (b) $a = -0.55$.

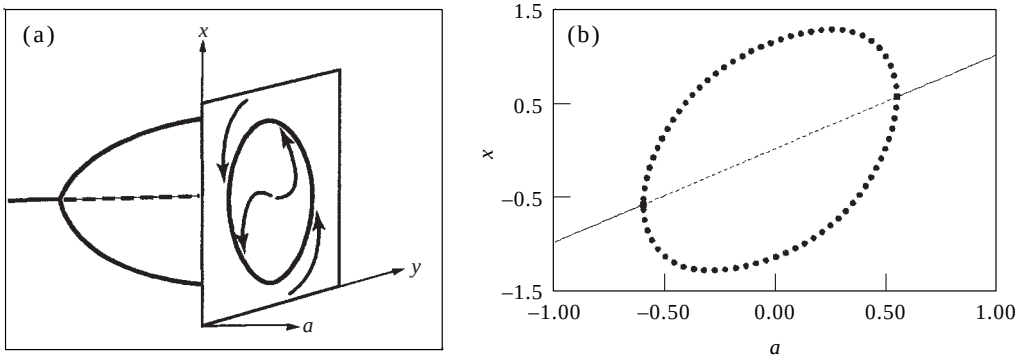

FIG. A2. Hopf bifurcation in eqn (*). As a increases (at fixed $b = 5$, $c = 0.1$ and $p = 1$), the steady state loses stability and a family of small amplitude, stable limit cycle solutions arises: (a) the envelope of these closed orbits traces out a paraboloid surface in three-dimensional space (x,y,a); (b) the amplitude of the limit cycle (x_{min} and x_{max}) is plotted as a function of a. Supercritical Hopf bifurcations occur at $a = -0.5905$ and $+0.5494$.

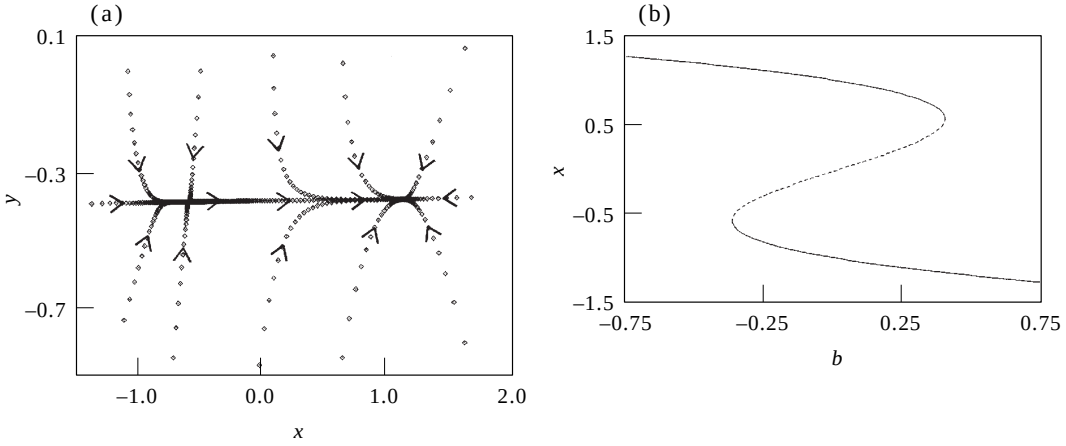

FIG. A3. Saddle-node bifurcation in eqn (*): (a) phase portrait ($a = -5.0$, $b = -0.36229$, $c = 0.1$, $p = 1$); (b) bifurcation diagram. As b increases (at fixed a, c and p), a new stable node is created, seemingly *ex nihilo*, in combination with a saddle point. As b increases further, the saddle point moves over and annihilates the original stable node.

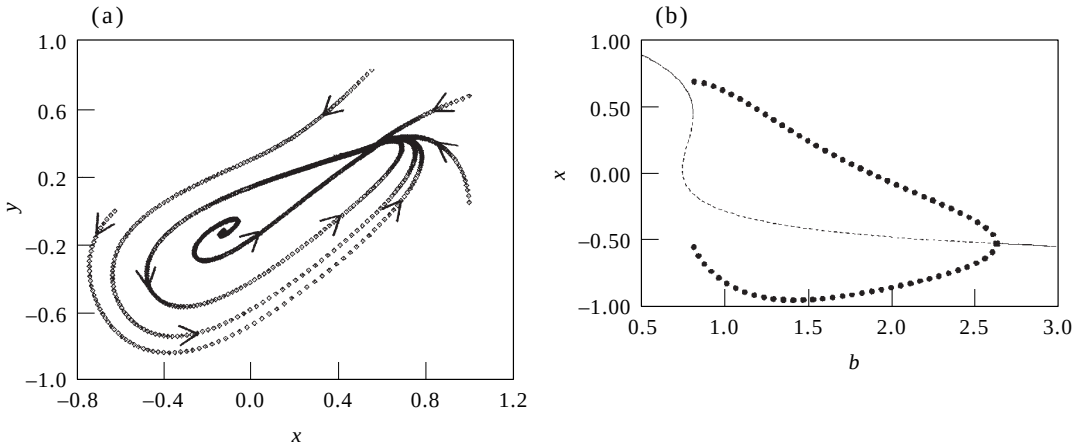

FIG. A4. Saddle-node on an invariant circle: (a) phase portrait ($a = -0.7$, $b = 0.81979$, $c = 0.53$, $p = 1$); (b) bifurcation diagram. As b increases (at fixed a, c and p), a saddle and node coalesce and are replaced by a stable limit cycle.

reaction term is an algebraic function of variables and "parameters", those rate constants and Michaelis constants that are necessary to describe how fast biochemical reactions proceed.

For simplicity, let us suppose we have a system described by two variables (x and y) and four parameters (a, b, c and p):

$$\begin{aligned} \frac{dx}{dt} &= f(x,y;p) = p[x(1-x^2)-y] \\ \frac{dy}{dt} &= g(x,y;a,b,c) = (x-a)(b-y)-c \end{aligned} \qquad (*)$$

We have chosen specific functions, f and g, for illustrative purposes only. They do not represent a biochemical control system because the variables and parameters are allowed to take on negative values (i.e. they are not concentrations and rate constants). For a given set of parameters values, if we specify initial conditions, $x(0) = x^0$ and $y(0) = y^0$, then we can solve the DEs numerically to obtain two functions, $x(t)$ and $y(t)$, that describe exactly how the system evolves in time. For instance, the dynamical system may approach a stable steady state: $x(t) \to x^*$ and $y(t) \to y^*$, as $t \to \infty$ (here, x^* and y^* are constants). Or it may approach a stable (limit cycle) oscillation: $x(t) \to x_{per}(t)$ and $y(t) \to y_{per}(t)$, as $t \to \infty$ [here, $x_{per}(t)$ and $y_{per}(t)$ are periodic functions of minimal period T]. These ideas are illustrted in Fig. A1, where we plot solutions of eqn (*) as trajectories in state space (also called the "phase" plane).

The qualitative appearance of trajectories in the phase plane is called the "phase portrait" of the system. In Fig. A1 all trajectories are sucked into a single stable steady state for a small; whereas, for larger values of a, trajectories leave an unstable steady state and are attracted to a stable limit cycle. At some intermediate value of a (called the bifurcation point), the system must make a smooth transition from one phase portrait to the other. The bifurcation is illustrated schematically in Fig. A2(a). In eqn (*), as a increases through a^H, the steady state loses stability and a family of small amplitude, stable limit cycles is born [see Fig. A2(b)]. This is called a supercritical Hopf bifurcation. At a subcritical Hopf bifuration (not shown), an unstable steady state gains stability and a family of small amplitude, unstable limit cycles is born.

Equations (*) can also illustrate a saddle-node bifurcation (Fig. A3) and a SNIC bifurcation (Fig. A4). In the latter case, a saddle-node bifurcation occurs on an invariant circle [Fig. A4(a)], which is a closed trajectory that proceeds out of the saddle-node and then swings around to come back into the saddle-node in a different direction as $t \to \infty$. Beyond the SNIC bifurcation, the system has a stable limit cycle of long period [Fig. A4(b)].